Journal of Inflammation Research

Dovepress
Taylor & Francis Group

Open Access Full Text Article

ORIGINAL RESEARCH

Pharmacological Mechanisms of CheReCunJin Formula in Ameliorating Sjögren's Syndrome: Suppression of IL-17 Signal-Mediated Inflammatory Cascade

Yu Gan[1,2], Lijing Du[2,3], Yuanfang Sun[2,3], Fugen Li[2], Haoran Chen[2], Shikai Yan[3], Xue Xiao[4], Shasha Li[2,*], Bin Wu[1,*]

[1]Department of Rheumatology, Chongqing Traditional Chinese Medicine Hospital, Chongqing, People's Republic of China; [2]The Second Clinical College, Guangzhou University of Chinese Medicine, Guangzhou, Guangdong, People's Republic of China; [3]School of Pharmacy, Shanghai Jiao Tong University, Shanghai, People's Republic of China; [4]Institute of Traditional Chinese Medicine, Guangdong Pharmaceutical University, Guangzhou, Guangdong, People's Republic of China

*These authors contributed equally to this work

Correspondence: Bin Wu; Shasha Li, Email wuubinn@126.com; happylishasha@163.com

Background: Sjögren's Syndrome (SS) is the second most prevalent autoimmune disease in China without effective therapy. Current evidence indicates safety and effectiveness of CheReCunJin formula (CRCJ) in treating SS. However, the underlying mechanism remains unclear.

Methods: UPLC-Q-TOF-MS was applied for compound identification. Multiple components, targets and pathways involved in the treatment of SS with CRCJ were predicted by network pharmacology. Molecular docking was used for preliminary validation. NOD mouse, a classic spontaneous SS model, was used to examine the therapeutic effects on SS of CRCJ. The potential mechanism of CRCJ to mitigate SS was investigated by serum untargeted metabolomics. Validation of key pathway and targets was conducted using flow cytometry, ELISA, immunohistochemistry, Masson staining, and Western blot.

Results: 373 compounds were identified in CRCJ. Through network pharmacology and molecular docking, 15 main components (eg, luteolin 7-O-β-D-glucoside, rutin, 1,4-dicaffeoylquinic acid, anemarsaponin C), 10 core targets (including HSP90AA1, TNF, MMP9, MAPK1, IL6), and the key pathway for CRCJ treating SS, IL-17 signaling pathway, were screened out. In NOD mice, CRCJ demonstrated the ability to improve salivary flow rate and water intake, reduce submandibular gland (SMG) tissue damage, and diminished the levels of IFN-α, IFN-β, IgG in serum. CRCJ modulated metabolic disorders, differentially regulating 63 metabolites and 6 metabolic pathways. Additional validation showed that CRCJ inhibited the Th17 cell activation, downregulated IL-17 signal transduction, and improved ECM degradation in SMG.

Conclusion: CRCJ protected salivary glands in SS by inhibiting IL-17 signal-mediated inflammatory cascade, an effect likely attributable to key bioactive components such as luteolin 7-O-β-D-glucoside, rutin, 1,4-dicaffeoylquinic acid, and anemarrhenasaponin C. This study provides a foundation for the further development and clinical application of CRCJ for the treatment of SS.

Keywords: CheReCunJin formula, IL-17 signal pathway, inflammatory cascade, metabolomics, network pharmacology, Sjögren's syndrome

Introduction

Sjögren's syndrome (SS) is a chronic progressive autoimmune disease (AID), divided into primary SS (pSS) and secondary SS. Based on evidence from large population studies, the most recent estimates of the global prevalence of pSS range from 0.01% to 0.05%.[1] However, the prevalence of pSS is 0.33%–0.77% and pSS is the second largest AID in China.[2,3] The presence of focal infiltrates composed of autoreactive lymphocytes, with associated tissue injury at the

Received: 5 June 2025
Accepted: 2 December 2025
Published: 10 December 2025

level of the exocrine glands, is one of its typical features.[4] Invasion of the salivary glands is characterized by dry mouth, one of its most prevalent symptoms.[5] It affects food chewing and swallowing, and oral complications such as dental caries and candidiasis occur.[5] In severe cases, multiple organ and systemic damage occurs even concurrently with lymphoma and is life-threatening.[6] Therefore, SS can be considered an enormous social and economic burden with a high impact on patients' quality of life.

At present, there is still no ideal treatment plan or specific drug for SS. Oral sicca symptoms are usually treated symptomatically with muscarinic agonists, such as pilocarpine and cevimeline, to stimulate salivary gland secretion. Saliva substitutes are applied to keep the mouth moist.[6,7] There is a lack of convincing evidence for the use of conventional synthetic disease-modifying anti-rheumatic drugs (DMARDs) or biologic DMARDs for the management of systemic complications.[8] The effectiveness of hydroxychloroquine (HCQ) also needs to be further evaluated, even though it is the most widely used drug in the clinic.[7]

With the advantages of curative effects, fewer adverse effects, and lower prices, TCM is increasingly being used to improve symptoms and slow the progression of SS.[9,10] The *CheReCunJin formula* (CRCJ), which is a combination of twelve Chinese medicines, has been used clinically for the treatment of SS for more than ten years. Together, they serve to clear heat, purge fire, tonify qi, and nourish yin. Evidence from our clinical study suggests that CRCJ is efficacious in increasing salivary production, improving disease activity and symptom severity scores, and alleviating autoimmune inflammation in SS patients.[11] However, despite these clinical benefits, the specific bioactive components of CRCJ and the molecular mechanisms by which it ameliorates autoimmune inflammation in SS are poorly defined, representing a critical knowledge gap that hinders rational development and wider clinical translation.

To address this knowledge gap, we first employed UPLC-Q-TOF-MS to characterize chemical constituents in CRCJ. Network pharmacology and molecular docking were applied to investigate the active components, core targets and key pathway mediating therapeutic effects. Subsequently, NOD mice modeling SS manifestations were monitored for body weight fluctuations and water consumption, while salivary flow rate, submandibular gland (SMG) histopathology, serum IFN and IgG levels were determined to assess CRCJ efficacy. In addition, untargeted metabolomics revealed differential metabolites and associated pathways underlying CRCJ's therapeutic action. To confirm the crucial targets and mechanisms identified by network pharmacology and metabolomics, experimental validation using flow cytometry, ELISA, immunohistochemistry, Masson staining, and Western blotting were conducted (Supplementary Figure S1).

Materials and Methods

Drugs and Preparations

The 12 kinds of Chinese herbal medicine included in CRCJ were supplied by Guangdong Provincial Hospital of Chinese Medicine (Table 1). The TCM decoction method was used to prepare the CRCJ: 1) add 260 g of the crude drugs and 2080 mL of water (1:8, w/v) to a casserole; 2) boil over high heat after soaking for 30 min; 3) decoct for 40 minutes over moderate heat; 4) filter with eight layers of gauze, and then pour out the medicinal liquid; 5) stir in 1560 mL of water (1:6, w/v) and repeat steps 2) - 4); and 6) mix the two filtrates.

Compound Characterization of CRCJ

UPLC-Q-TOF-MS was used to collect chemical component information of CRCJ (0.21g/mL) in positive and negative ion modes. Sample separation was carried out on a Waters CORTECS UPLC T3 column (2.1 × 100 mm, 1.6 μm) maintained at 20°C. The mobile phase consisted of methanol (A) and ultrapure water containing 0.1% formic acid (B). The gradient elution program: 0–3 min, 2% (A) → 2% (A); 3–23 min, 2% (A) → 98% (A); 23–25 min, 98% (A) →98% (A). The injection volume was 5 μL, while the elution flow rate was 0.2 mL/min. The settings were applied: ion spray voltage of 5500 V/-4500 V, collision energy of 10 V (MS) and 35V (MS/MS), source temperature of 500°C, curtain gas at 35 psi, and gas 1 and gas 2 both at 50 psi. The raw data was imported into PeakView software for processing. Based on retention time, precise molecular weight, structure, MS/MS fragments, etc, CRCJ compounds were identified by comparing the information with that collected from TCMSID (https://tcm.scbdd.com/home/search_index/), ETCM (http://www.tcmip.cn/ETCM/index.php/Home/Index/index.htmL), TCMSP (https://tcmsp-e.com/index.php), and literature.

Table 1 Composition Information of CRCJ

Chinese Name	Pharmaceutical Name	Botanical Information	Weight (g)
Shigao	Gypsum Fibrosum	Sulfate mineral anhydrite gypsum, mainly containing hydrated calcium sulfate ($CaSO_4 \cdot 2H_2O$)	30
Zhimu	Anemarrhenae Rhizoma	Dried rhizome of Liliaceae plant Anemarrhena asphodeloides Bge.	15
Xiakucao	Prunellae Spica	Dried ear of Labiatae plant Prunella vulgaris L.	15
Lugen	Phragmitis Rhizoma	Fresh or dried rhizome of Gramineae plant Phragmites communis Trin.	30
Gegen	Puerariae Lobatae Radix	Dried root of Leguminosae plant Pueraria lobata (Willd.) Ohwi	15
Sangye	Mori Folium	Dried leaf of Moraceae plant Morus alba L.	10
Juhua	Chrysanthemi Flos	Dried capitulum of Compositae plant Chrysanthemum morifolium Ramat.	10
Huangqi	Astragali Radix	Dried root of Leguminosae plant Astragalus membranaceus (Fisch.) Bge. var. mongholicus (Bge.) Hsiao or Astragalus membranaceus (Fisch.)Bge.	60
Dihuang	Rehmanniae Radix	Fresh or dried root tuber of Scrophulariaceae plant Rehjnannia glutinosa Libosch.	15
Maidong	Ophiopogonis Radix	Dried root tuber of Liliaceae plant Ophiopogon japonicus (L. f) Ker-Gawl.	15
Beishashen	Glehniae Radix	Dried root of Umbelliferae plant Glehnia littoralis Fr. Schmidt ex Miq.	30
Niuxi	Achyranthis bidentatae radix	Dried root of Amaranthaceae plant Achyranthes bidentata Bl.	15

Network Pharmacology and Molecular Docking

The targets of the CRCJ compounds were collected from TCMSP, ETCM, Super-PRED (https://prediction.charite.de/subpages/target_prediction.php), and SwissTargetPrediction (http://www.swisstargetprediction.ch/). SS targets were collected through GenCards, DisGeNET (https://www.disgenet.org/), OMIM (https://omim.org/), TTD (http://db.idrblab.net/ttd/), and DrugBank (https://go.drugbank.com/). The protein-protein interaction (PPI) network of their intersecting targets was constructed in STRING 12.0 at the highest confidence level, excluding independent nodes. Subnetworks and Top10 targets of PPI were uncovered utilizing Cytoscape 3.10.1. GO functional annotation and KEGG pathway enrichment analysis were performed on targets with degree values ≥ 10 at Metascape 3.5 platform (https://metascape.org/gp/index.htmL#/main/step1). The compound-target-Top10 pathway network was further constructed to screen the active components and core targets.

AutoDock Vina 1.1.2 (http://autodock.scripps.edu/) was applied to predict the binding affinity of active components to core targets. The binding energy less than −5 kcal/mol was considered to have good binding affinity. The pairs with the best binding affinities were visualized using PyMOL software.

Animals and Interventions

Specific pathogen-free 8-week-old NOD/ShiLtJ female mice (20 ± 2 g, n = 36) and age- and sex-matched ICR mice (30 ± 2 g, n = 12) were obtained from Chang Zhou Cavens Laboratory Animal Ltd. (animal quality certificate number: 320730221100034153 and 99001700026182), eating and drinking freely. The experimental protocol followed the Guide for the Care and Use of Laboratory Animals and was approved by the Ethical Committee of Guangdong Provincial Hospital of Chinese Medicine (The Second Clinical College of Guangzhou University of Chinese Medicine, Guangzhou, China; approval number: 2022063). NOD mice were randomly divided into three groups: MOD group (drinking water, 10 mL/kg/d), HCQ group (Fenle, 0.052 g/kg/d), and CRCJ group (16.9 g/kg/d, equivalent to the crude herb). ICR mice were used as the control

(CON) group. The dose conversion procedure between 70 kg adults and mice was performed. Each group underwent seven weeks of continuous gavage.

Measurement of Salivary Flow Rate and Daily Water Consumption

Before and after 7-week administration, the mice were subjected to 5% chloral hydrate (200 mg/kg, i.p.) for sedation. Whole saliva was collected for 15 min from the oral cavity after the injection of pilocarpine nitrate (2 mg/kg, i.p). Saliva flow rates were expressed as microliters of saliva secreted per min per gram body weight (μL/min/g). To quantify daily water consumption, the remaining water in each cage's bottle was measured at a fixed time every other day.

Collection of Samples

The eyeballs were removed for blood collection under 20% urethane anesthesia (800 mg/kg, i.p). Blood, spleens, thymuses, and submandibular glands (SMGs) were gathered for later studies. The organ index was calculated as organ weight (mg)/ body weight (g).[12] The CON group was excluded from the between-group comparisons because of the significant influence of germline differences on organ index.

Histopathological Analysis

The SMG tissues were dehydrated and embedded in paraffin after 48 h of fixation in 4% paraformaldehyde. The wax blocks were cut into 5-μm sections for HE and Masson staining. The number of lymphocytic infiltration focus (an aggregate of 50 or more lymphocytes and histiocytes) and the area lymphocytic infiltration in SMG were analyzed.[13] SMG injury degree was assessed according to the grading standard from Cutler.[14]

Serum Untargeted Metabolomics

UPLC-Q-TOF-MS Analysis

The serum samples were analyzed using a Waters Acquity UPLC system (Waters, Milford, MA, USA) coupled to a Q-TOF-MS (TripleTOF® 5600 + System, AB SCIEX, Framingham, MA, USA). Sample separation was carried out on an Acquity UPLC BEH C18 column (2.1 × 100 mm, 1.7 μm) maintained at 30°C. The gradient elution program was performed with ultrapure water containing 0.1% formic acid (A) and methanol (B) as the mobile phase: 0–5 min, 95% (A) → 68% (A); 5–17 min, 68% (A) → 36% (A); 17–25 min, 36% (A) →15% (A); 25–33 min, 15% (A) → 5% (A); and 33~48 min, 5% (A). The injection volume was 5 μL, while the elution flow rate was 0.3 mL/min. Pooled QC samples were prepared by mixing equal amounts of serum from each sample and tested using the same procedure.

Mass spectrometry was performed with an electrospray ionization source applied in positive ion mode. The following source settings were applied: ion spray voltage of 5500 V, collision energy of 10 V (MS) and 40V (MS/MS), source temperature of 500°C, curtain gas at 35 psi, and gas 1 and gas 2 both at 50 psi.

Data Processing and Analyzing

Raw data were processed using Progenesis QI software (Waters, Milford, MA, USA). QC sample data was selected as a reference. The metabolites were identified based on accurate molecular mass, tandem mass data, and the human metabolome database (HMDB). PCA and PLS-DA were performed using SIMCA 14.1. Metabolites with VIP value >1, p-value < 0.05, and fold change (FC) value <0.5 or >2 was <0.5 or FC>2 was retained as differentially expressed metabolites.[15,16] The differential metabolites were imported into MetaboAnalyst 6.0 (https://www.metaboanalyst.ca/) for the Kyoto Encyclopedia of Genes and Genomes (KEGG) pathway enrichment analysis.

Flow Cytometry for Th17 Cells

Single-cell suspensions of the spleens were prepared through a 200-mesh filter. The resuspended cells were stimulated with a BFA/Monensin mixture and a PMA/Ionomycin mixture (Multisciences, Hangzhou, China) for five hours at 37°C in a 5% CO_2 environment after lysis of erythrocytes. The cells were incubated with a FITC-labeled anti-mouse CD3 antibody (Elabscience, clone 17A2) and a PE-Cy7-labeled anti-mouse CD4 antibody (BioLegend, Cat#100422) for 30 min, fixed and permeabilized with a Foxp3/Transcription Factor Staining Buffer Set (eBioscience, San Diego, CA,

USA), and stained intracellularly with a PE-labeled anti-IL-17A antibody (eBioscience, clone eBio 17B7) for 30 min to sort Th17 cells. The sample data were acquired by NovoCyte Quanteon flow cytometry and analyzed by NovoExpress software (Agilent, Santa Clara, CA, USA).

Elisa

The serum levels of interferon (IFN)-α, IFN-β, IgG, IL-17, IL-6, TNF-α, and desmosine were detected by ELISA kits (Enzyme-linked Biotechnology, Shanghai, China). The kits were equilibrated to room temperature for 30 min before the assay. The operation was conducted following the kit instructions, and the content was analyzed by measuring the absorbance of the sample at 450 nm.

Immunohistochemistry (IHC)

IHC was conducted following the instructions of the IHC kits. The sample sections were incubated overnight at 4°C with primary antibodies against IL-17A (Proteintech, 26163-1-AP, 1:200) and matrix metalloproteinase-9 (MMP-9; Servicebio, GB11132-100, 1:200). Following subsequent incubation with anti-rabbit lgG-HRP for 1 h at 37°C, the color was developed with diaminobenzidine chromogen solution. Representative images from each slide were viewed through an optical microscope. The regions with positive expression were analyzed using ImageJ.

Western Blotting (WB)

The proteins extracted from SMG were separated by SDS-PAGE and then transferred onto PVDF membranes based on the molecular weight. After blocking with 5% non-fat milk for 1 h, the membranes were incubated overnight with primary antibodies: anti-IL-17RA (Bioss, bs-2606R, 1:2000), anti HSP90 (CST, 4877T, 1:1000), anti-Act1 (abclonal, A6776, 1:1000), anti-TRAF6 (Abcam, ab40675, 1:2000), anti-p-ERK (CST, 4370S, 1:1000), anti-ERK (CST, 4695S, 1:1000), and anti-tubulin (CST, 2125S, 1:2000). Then, the membranes were incubated with anti-rabbit secondary antibody (CST, 7074S, 1:4000) prior to automated chemiluminescence visualization. The images of target proteins were analyzed using ImageJ.

Statistical Methods

GraphPad Prism 9 software was used for statistical processing and analysis. The data are shown as mean ± standard error of mean (SEM). First, a normality test was conducted on the data. When the data conformed to a normal distribution, one-way ANOVA was used to compare multiple groups. Tukey's multiple comparisons test was used for between-group comparisons if homoscedasticity was met, and Dunnett's T3 multiple comparisons test was used if it was not met. Failure to conform to a normal distribution was tested using the Kruskal–Wallis test. The test level was bilateral $\alpha = 0.05$, and p-value < 0.05 indicated a statistically significant difference.

Results

Compound Identification of CRCJ

The fingerprint spectrums of CRCJ (Figure 1A) were obtained through UPLC-Q-TOF-MS (Figure 1B and C). A total of 373 compounds were identified from the 11 herbs in CRCJ, including 104 flavonoids (27.88%), 69 terpenoids (18.5%), 36 organic acids (9.65%), and other compound categories (Figure 1D). The twelfth drug, Shigao, consists predominantly of hydrated calcium sulfate ($CaSO_4 \cdot 2H_2O$) and was not amenable to characterization by this method because of its physicochemical properties. Afzelin (No.109), neomangiferin (No. 111), puerarin (No.135), puerarin-6″-O-xyloside (No. 142), 1,4-dicaffeoylquinic acid (No. 201), and anemarsaponin C (No.268) exhibited high response intensities and relative contents. Compound serial number and details are shown in Supplementary Table S1.

Network Pharmacology Analysis

PPI Network Analysis

After databases search, 1530 targets of 373 compounds in CRCJ and 1257 targets of SS were collected, resulting in 249 intersecting targets (Figure 2A). A network of unique or shared components belonging to 11 herbs and intersecting

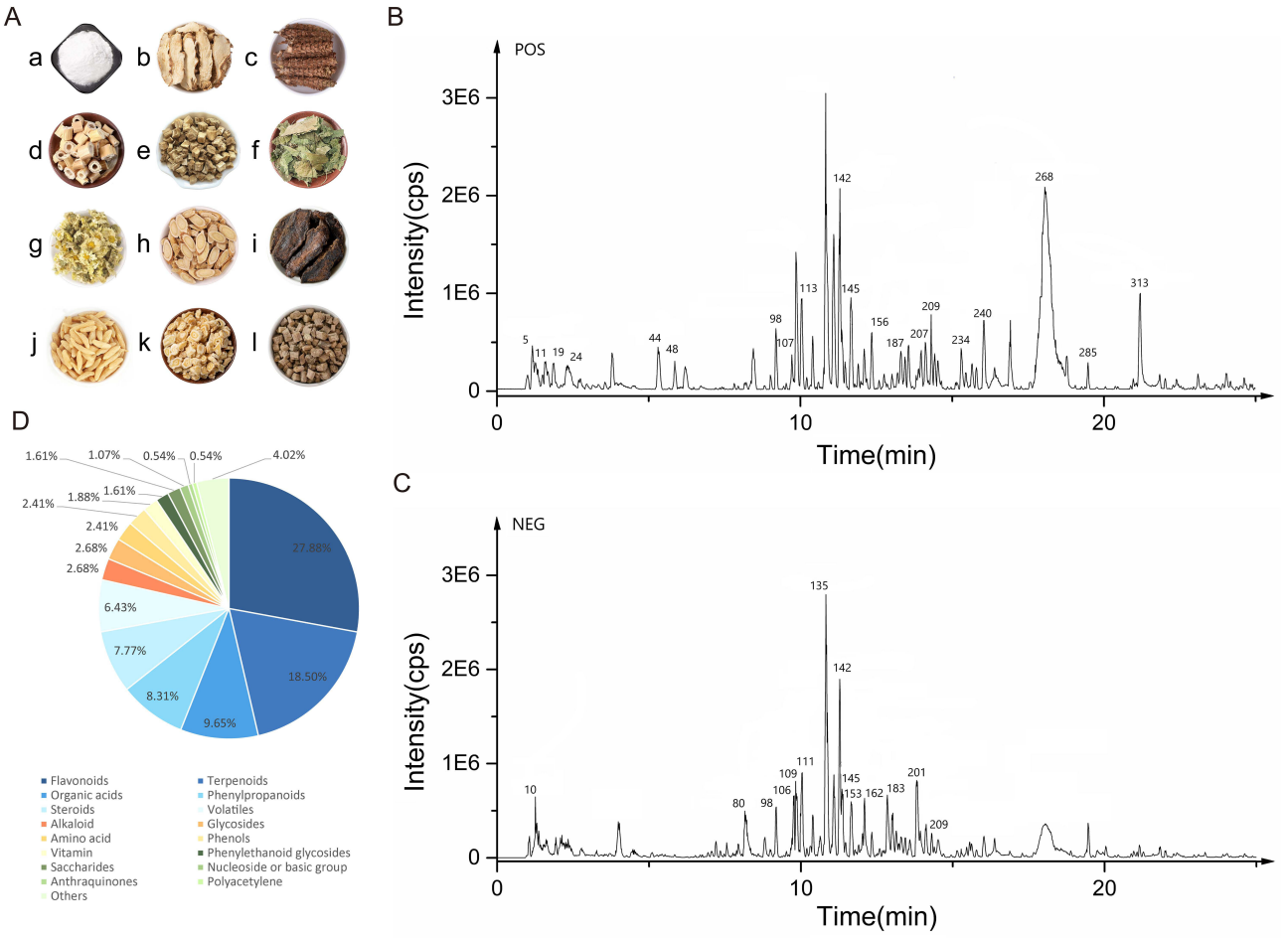

Figure 1 Compound analysis of CRCJ. (**A**) Crude drugs of CRCJ. a, Shigao; b, Zhimu; c, Xiakucao; d, Lugen; e, Gegen; f, Sangye; g, Juhua; h, Huangqi; i, Dihuang; j, Maidong; k, Beishashen; l, Niuxi. (**B** and **C**) The fingerprint spectrum of CRCJ in positive and negative modes. (**D**) Classification of compounds.

targets was constructed to show their interaction relationship (Figure 2B). PPI network consisted of 207 nodes and 831 edges (Figure 2C). 12 subnetwork modules were mined to gain more information (Table 2) and the top three were visualized (Figure 2D–F). CytoHubba plugin was used to obtain Top10 targets (Figure 2G) and their scores: TNF (42), TP53 (36), IL6 (34), IFNG (30), IL1B (30), AKT1 (29), STAT3 (27), NFKB1 (27), JUN (25), CXCL8 (24).

GO and KEGG Enrichment Analysis

Screening based on $P < 0.05$, GO biological processes enriched 1310 entries, cellular component involved 53 entries, while molecular function included 90 entries, suggesting CRCJ may affect pathological processes such as inflammatory response and immune cell activation in SS (Figure 2H). KEGG analysis enriched 159 signaling pathways, including IL-17 signaling pathway, NOD-like receptor signaling pathway, JAK-STAT signaling pathway, chemokine signaling pathway, and cytokine-cytokine receptor interaction, which were closely related to SS (Figure 2I).

The Component-Target-Top10 Pathway Network

The component-target-Top10 pathway network was constructed to screen for active components and core targets (Figure 2J). Quercetin, genistein, apigenin, luteolin, and kaempferol in CRCJ may regulate key signaling pathways in SS through core target genes such as HSP90AA1, TNF, NFKB1, EGFR, and PRKACA. Considering the compound intensity in UPLC-Q-TOF-MS and Top10 targets in PPI network, 15 active components (Table 3 & Supplementary Figure S2) and 10 core targets (Table 4) were ultimately determined.

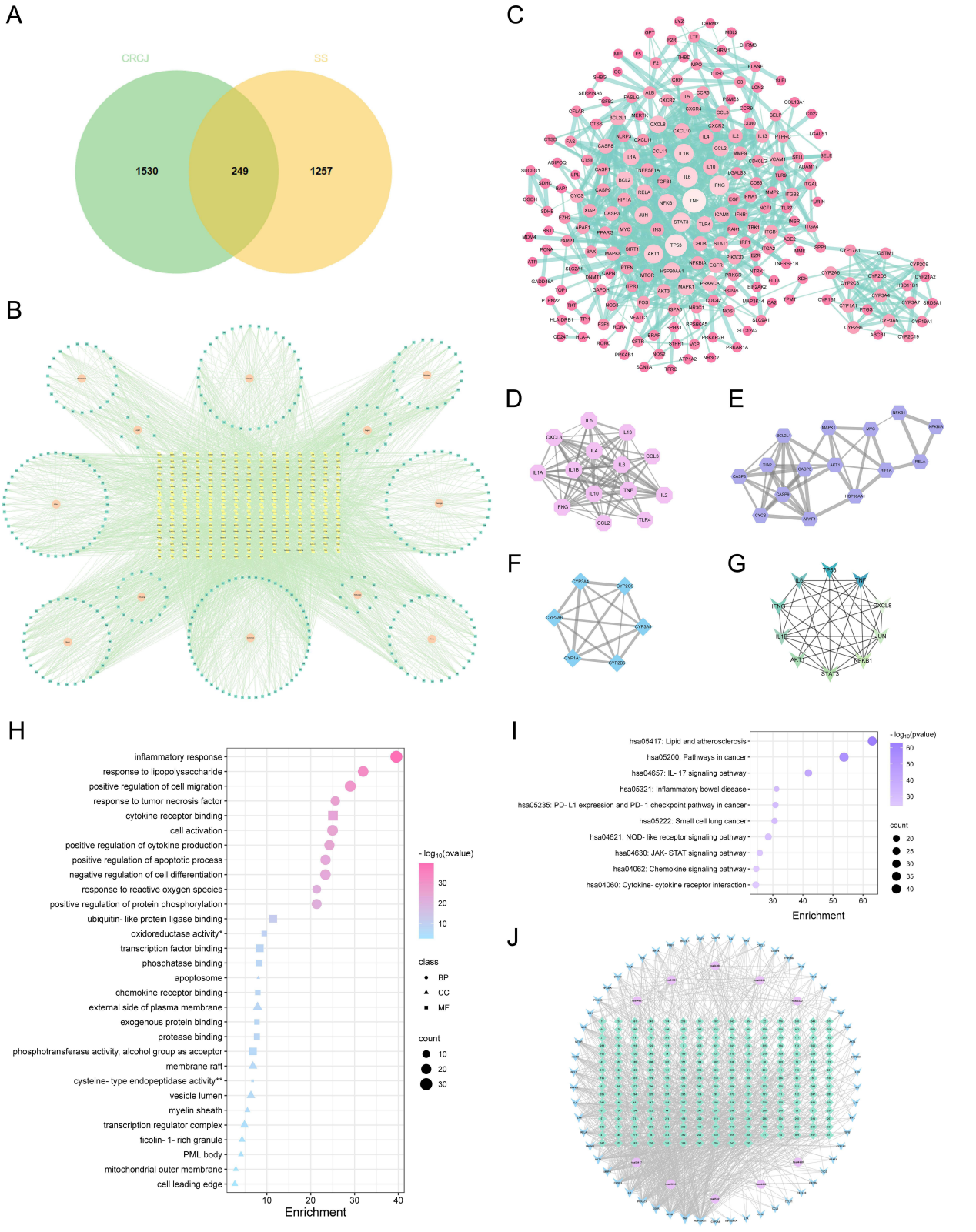

Figure 2 Network pharmacology analysis of CRCJ. (**A**) Venn diagram of the targets. (**B**) The network of 328 potential active components and 249 intersecting targets. (**C**) The PPI network. (**D**–**F**) Top3 subnetwork modules of PPI network. (**G**) Top10 targets of PPI network. (**H** and **I**) GO and KEGG enrichment analyses. (**J**) The active components-targets-Top10 pathway network. *oxidoreductase activity, acting on paired donors, with incorporation or reduction of molecular oxygen, reduced flavin or flavoprotein as one donor, and incorporation of one atom of oxygen. **cysteine-type endopeptidase activity involved in apoptotic signaling pathway.

https://doi.org/10.2147/JIR.S544874

Table 2 Subnetwork Modules of the PPI Network

No.	Targets	MCODE Score	Nodes	Edges
1	TNF, IL6, IL1B, TLR4, IFNG, CXCL8, CCL2, IL1A, IL10, IL4, IL2, CCL3, IL13, IL5	12.000	14	78
2	AKT1, MAPK1, NFKB1, HSP90AA1, RELA, CASP3, HIF1A, NFKBIA, BCL2L1, MYC, XIAP, CASP8, CYCS, CASP9, APAF1	6.000	15	42
3	CYP2A6, CYP1A1, CYP3A4, CYP2C9, CYP3A5, CYP2B6	6.000	6	15
4	SDHB, SDHC, SUCLG1, OGDH	3.333	4	5
5	NLRP3, CASP1, FAS, FASLG, CTSB, CTSS, CTSD, MPO, CFLAR, ELANE, CTSG, LTF, LYZ	3.167	13	19
6	STAT3, EGFR, BCL2, STAT1, MAPK8	3.000	5	6
7	JUN, TP53, FOS	3.000	3	3
8	E2F1, DNMT1, EZH2	3.000	3	3
9	IRAK1, TLR9, TLR7	3.000	3	3
10	HSPA8, GAPDH, HSPA5, CFTR, VCP, TPI1, TKT	3.000	7	9
11	CRP, PTPRC, CD40LG, CD80, CD86, ITGA4, ITGA2, ITGAL, SELP, C3, SELL, F2, SELE, GPT, MBL2, THBD, F2R, CHRM1, CHRM2	2.889	19	26
12	NOS1, NOS3, NOS2, XDH, TPMT, CYP3A7, CYP2D6, HSD11B1, CYP2C8, CYP2C19, CYP17A1, CYP19A1, PTGS1, CYP21A2, SRD5A1	2.714	15	19

Table 3 Active Components Used as Ligands for Molecular Docking

No.	Compound Name	Molecular Formula	Intensity in LC/MS	Degree	BC	CC	ASPL	Crude Drug
1	Anemarsaponin C	C45H74O18	1,924,284	4	0.002	0.350	2.861	Zhimu
2	Puerarin	C21H20O9	790,723	15	0.011	0.382	2.616	Gegen
3	1,4-Dicaffeoylquinic acid	C25H24O12	599,675	3	0.000	0.288	3.470	Juhua
4	Afzelin	C21H20O10	578,887	2	0.000	0.308	3.245	Zhimu
5	Calycosin 7-O-β-D-glucoside	C22H22O10	566,531	2	0.000	0.308	3.245	Huangqi
6	Rhamnocitrin 3-O-glucoside	C22H22O11	565,557	2	0.000	0.308	3.245	Huangqi
7	Adenosine	C10H13N5O4	562,101	4	0.001	0.317	3.159	Dihuang, Maidong, Beishashen
8	Daidzein 4′,7-diglucoside	C27H30O14	538,858	2	0.000	0.308	3.245	Gegen
9	Ononin	C22H22O9	488,941	2	0.000	0.308	3.245	Gegen, Huangqi
10	Diosmetin 7-O-β-D-glucoside	C22H22O11	444,882	4	0.002	0.350	2.854	Juhua
11	Luteolin 7-O-β-D-glucoside	C21H20O11	399,636	3	0.001	0.330	3.033	Xiakucao, Sangye, Juhua

(*Continued*)

Table 3 (Continued).

No.	Compound Name	Molecular Formula	Intensity in LC/MS	Degree	BC	CC	ASPL	Crude Drug
12	Rosmarinic acid	C18H16O8	290,695	13	0.009	0.372	2.689	Xiakucao
13	Caffeic acid	C9H8O4	170,414	1	0.000	0.284	3.523	Xiakucao, Lugen, Sangye, Juhua, Huangqi, Dihuang, Beishashen
14	Rutin	C27H30O16	136,790	6	0.001	0.325	3.073	Xiakucao, Sangye, Juhua, Huangqi, Beishashen, Niuxi
15	p-Hydroxycinnamic acid	C9H8O3	74,417	2	0.001	0.300	3.338	Xiakucao, Lugen

Abbreviations: BC, Betweenness Centrality; CC, Closeness Centrality; ASPL, Average Shortest Path Length.

Table 4 Core Targets Used as Receptors for Molecular Docking

No.	Target Name	PDB ID	Degree	BC	CC	ASPL
1	HSP90AA1	3O0I	80	0.198	0.437	2.288
2	TNF	2AZ5	74	0.143	0.430	2.328
3	NFKB1	8TQD	65	0.155	0.420	2.381
4	EGFR	3POZ	58	0.101	0.409	2.447
5	IL2	1M47	50	0.083	0.395	2.533
6	CASP3	1NME	47	0.068	0.397	2.520
7	MMP9	1L6J	44	0.074	0.399	2.507
8	AKT1	3MVH	42	0.089	0.396	2.526
9	MAPK1	1TVO	35	0.064	0.395	2.533
10	IL6	1ALU	29	0.035	0.388	2.579

Abbreviations: BC, Betweenness Centrality; CC, Closeness Centrality; ASPL, Average Shortest Path Length.

Molecular Docking

Molecular docking was performed to evaluate the binding affinity between active components and core targets. The best binding models and binding energies of every pair were obtained after nine docking attempts (Figure 3A). Out of 150 binding pairs, 40 pairs had binding energies ≤ −9 kcal/mol, while only two pairs had binding energies > −5 kcal/mol, indicating good binding affinities. In order to better showcase the binding structure, distinct four pairs of ligands and receptors at the lowest binding energy were visualized (Figure 3B–E). Every single active component tightly binded to different amino acid residues of the target proteins through several hydrogen bonds.

CRCJ Improved the Phenotype of SS Sialoadenitis

CRCJ Increased Salivary Secretion

The experimental process is presented in Figure 4A. The weight and water consumption of mice was monitored from 9 weeks of age (Figure 4B and C). Before administration, the salivary flow rate of NOD mice groups was significantly lower than that of the CON group (Figure 4D), suggesting salivary gland secretory dysfunction.[17] After 7 weeks of administration, the salivary flow rate of the MOD group further declined compared to the CON group, while the CRCJ

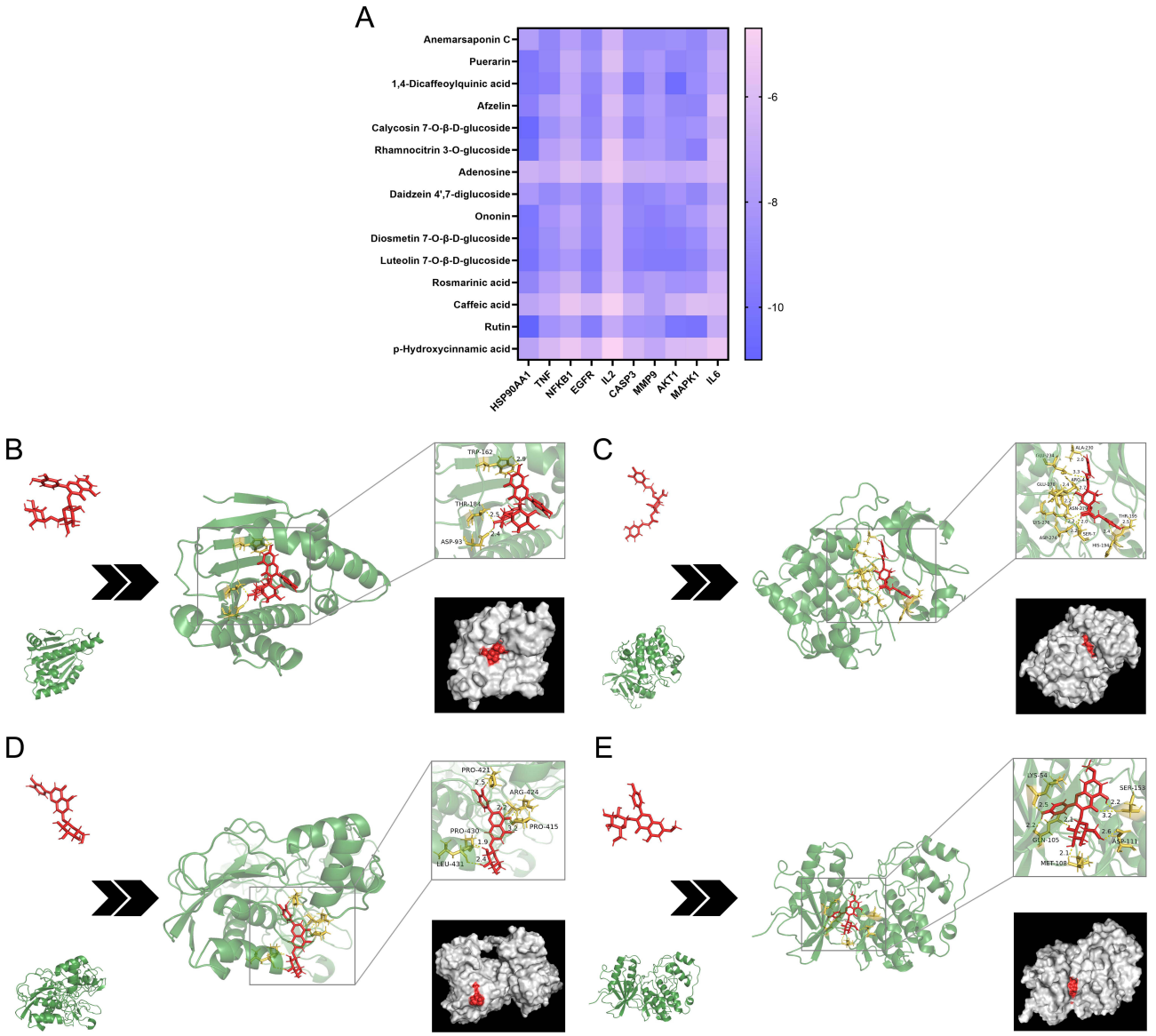

Figure 3 Results of molecular docking. (**A**) Heatmap of binding energy (kcal/mol). (**B**) Rutin and HSP90AA (−11 kcal/mol). (**C**) 1,4-Dicaffeoylquinic acid and AKT1 (−10.5 kcal/mol). (**D**) Luteolin 7-O-β-D-glucoside and MMP9 (−9.7 kcal/mol). (**E**) Rhamnocitrin 3-O-glucoside and MAPK1 (−9.4 kcal/mol).

group and HCQ group increased compared to the MOD group (Figure 4D). The results indicated the therapeutic potential of CRCJ for alleviating dry mouth. Detailed dataset is provided in Supplementary Table S2.

CRCJ Inhibited Autoimmunity

Autoimmune inflammation induces elevated SMG and immune organ coefficients in SS mice.[12,18,19] We found a slight decreasing trend of the SMG, thymus, and spleen index in the HCQ and CRCJ group compared to the MOD group (Figure 4E–G). Due to the activation of both innate and adaptive immune pathways, prominent IFN signatures were identified in SS with immunoglobulin production.[20] HCQ has been reported to improve SS by inhibiting the type I IFN (IFN-I) pathway and downregulating IgG level.[7] Our results showed that compared to the positive control drug, CRCJ exhibited greater advantages in reducing serum IFN-α, IFN-β, and IgG concentrations (Figure 4H–J).

CRCJ Mitigated Tissue Damage in SMG

Under light microscopy, the SMG tissue from CON group mice displayed intact, clear ductal structures, no lymphocytic infiltration foci, and neatly arranged follicles of uniform size (Figure 4K). By contrast, MOD group SMGs exhibited

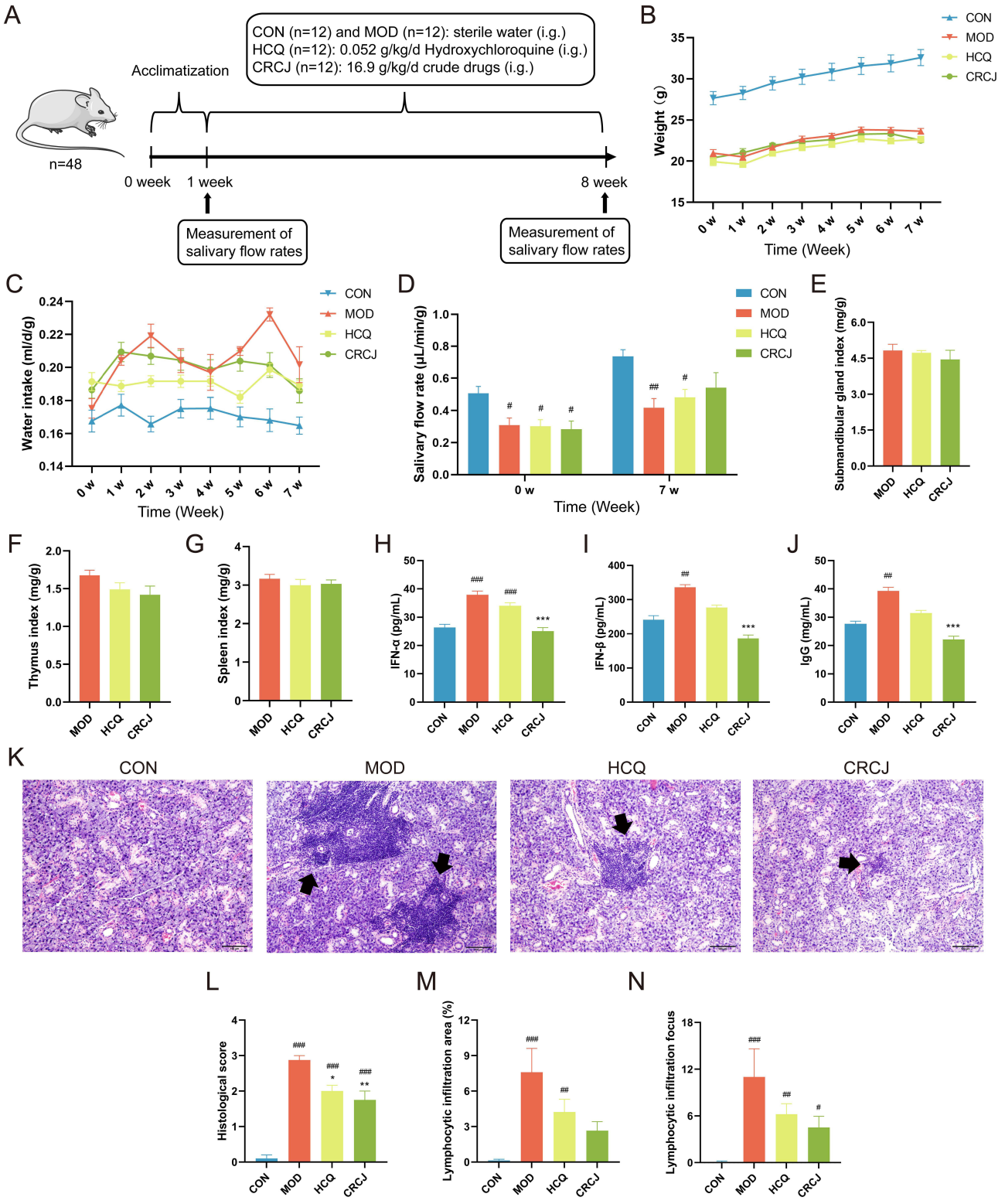

Figure 4 Multi-index evaluation on CRCJ treating SS. (**A**) The experimental procedures with mice. (**B**) Changes in body weight. (**C**) Changes in daily water intake. (**D**) Salivary flow rate before and after administration. (**E**–**G**) The ratio of weight of the bilateral SMGs, thymus, and spleen (mg) to body weight (g). (**H**–**J**) Serum IFN-α, IFN-β, and IgG levels in each group. (**K**) H&E staining showing pathological injuries (100× magnification). The black arrows show lymphocytic infiltration foci. (**L**) SMG damage was quantified according to the 1991 Cutler scoring system. (**M**) The area of lymphocytic infiltration. (**N**) The number of lymphocytic infiltration focus. w: week. $^{\#}$, $^{*}P<0.05$, $^{\#\#}$, $^{**}P<0.01$, $^{\#\#\#}$, $^{***}P<0.001$. $^{\#}$Compared with the CON group. *Compared with the MOD group.

https://doi.org/10.2147/JIR.S544874

multifocal lymphocytic infiltration (predominantly around ducts and blood vessels), accompanied by hyperplastic, disorganized ductal epithelial cells, variably dilated and distended glandular follicles, and scattered interstitial lymphocytic infiltration that disrupted the glandular structure. Compared to the MOD group, the number of histological score, lymphocytic infiltration area, and lymphocytic infiltration focus in the HCQ group and CRCJ group were diminished (Figure 4L–N).

CRCJ Regulated Metabolic Disorders in NOD Mice

The Regulation of Serum Metabolites by CRCJ

The serum metabolite profiles of the CON, MOD, and CRCJ group were subjected to pattern recognition. Both principal component analysis (PCA) and partial least squares siscriminant analysis (PLS-DA) showed that the three groups were distinguishable from each other (Figure 5A–C). The cross-validation results indicated that the model is well-fitted, highly predictable, and applicable (Figure 5D). Following the published screening methods, 63 differential endogenous metabolites were identified, with 46 upregulated and 17 downregulated by CRCJ, respectively (Figure 5E–G & Supplementary Table S3). [16,21] Notably, CRCJ upregulated LysoPC, 19,20-DiHDPA, and ursodeoxycholic acid 3-sulfate, which have anti-inflammatory effects.[22–26] CRCJ downregulated desmosine, a marker of ECM component degradation.[27–29] An increase in ECM degradation in exocrine glands has been found to correlate with SS pathogenesis.[30,31]

The Regulation of Metabolic Pathways by CRCJ

KEGG pathway enrichment analysis was conducted to gain further insights into the functional impact of altered metabolites on the progression and mitigation of SS. The 63 metabolites were enriched in 14 different pathways, among which -log(p) > 1 or pathway impact > 0.1 were significantly affected by CRCJ (Figure 5H and Table 5). Alpha-linolenic acid metabolism and linoleic acid metabolism were associated with immunity and inflammation, and upregulation of pentose and glucuronate interconversions pathway is positively correlated with increased Th17 cells in SS, which play an important role in the pathogenesis of SS.[32–34] Induced metabolic abnormalities in NOD mice exacerbate SS by increasing IL-17-producing cells.[17]

CRCJ Inhibited IL-17 Signal-Mediated Inflammatory Cascade

CRCJ Downregulated Th17/IL-17- Triggered Inflammation

Network pharmacology and metabolomics consistently linked CRCJ's mechanism to inhibiting Th17 activation and IL-17-mediated inflammatory cascades, including ECM degradation. To verify this, we first assessed splenic Th17/CD4+ T cell ratios, which were higher in the MOD group but lower in the CRCJ group (Figure 6A and B). IHC showed IL-17A was abundant in both the nucleus and cytoplasm of SMG in the MOD group (Figure 6C). The expression of IL-17A was significantly decreased in the CRCJ group (Figure 6D). The serum levels of IL-17, IL-6, and TNF-α in the CRCJ group were also decreased compared with the MOD group (Figure 6E–G). IL-17 activates the IL-17 signaling pathway and further activates MAPK signaling pathway. As verified by WB, the protein expression of IL-17RA, Act1, HSP90, and TRAF6 as well as ERK phosphorylation levels in SMG were significantly reduced in the group compared with the MOD group (Figure 6H–M), suggesting that CRCJ inhibited IL-17 signaling pathway transduction.

CRCJ Against ECM Degradation in SMG

Metabolomics detected altered serum desmosine concentrations in NOD mice, and ELISA confirmed that CRCJ reduced elevated desmosine levels (Figure 7A). Masson staining highlighted collagen fibers as blue-purple, another main ECM component (Figure 7B).[27,35] In the MOD group, inflammatory infiltration significantly occupied and destroyed normal perivascular and periductal collagen fibers; instead, reduced inflammatory infiltration resulted in damage mitigation in the HCQ and CRCJ groups. High expression of IL-17 promotes the production of MMP-9, which hydrolyzes ECM proteins, thus continually exacerbating acinar injury.[36–38] As shown by IHC staining, MMP-9 was mainly expressed in mucous acini and ducts (Figure 7C). The expression of MMP-9 was significantly decreased in the CRCJ group compared with the MOD group (Figure 7D). Consequently, ECM degradation was present in SMG and CRCJ may mitigate the pathological process by reducing MMP-9 production in NOD mice.

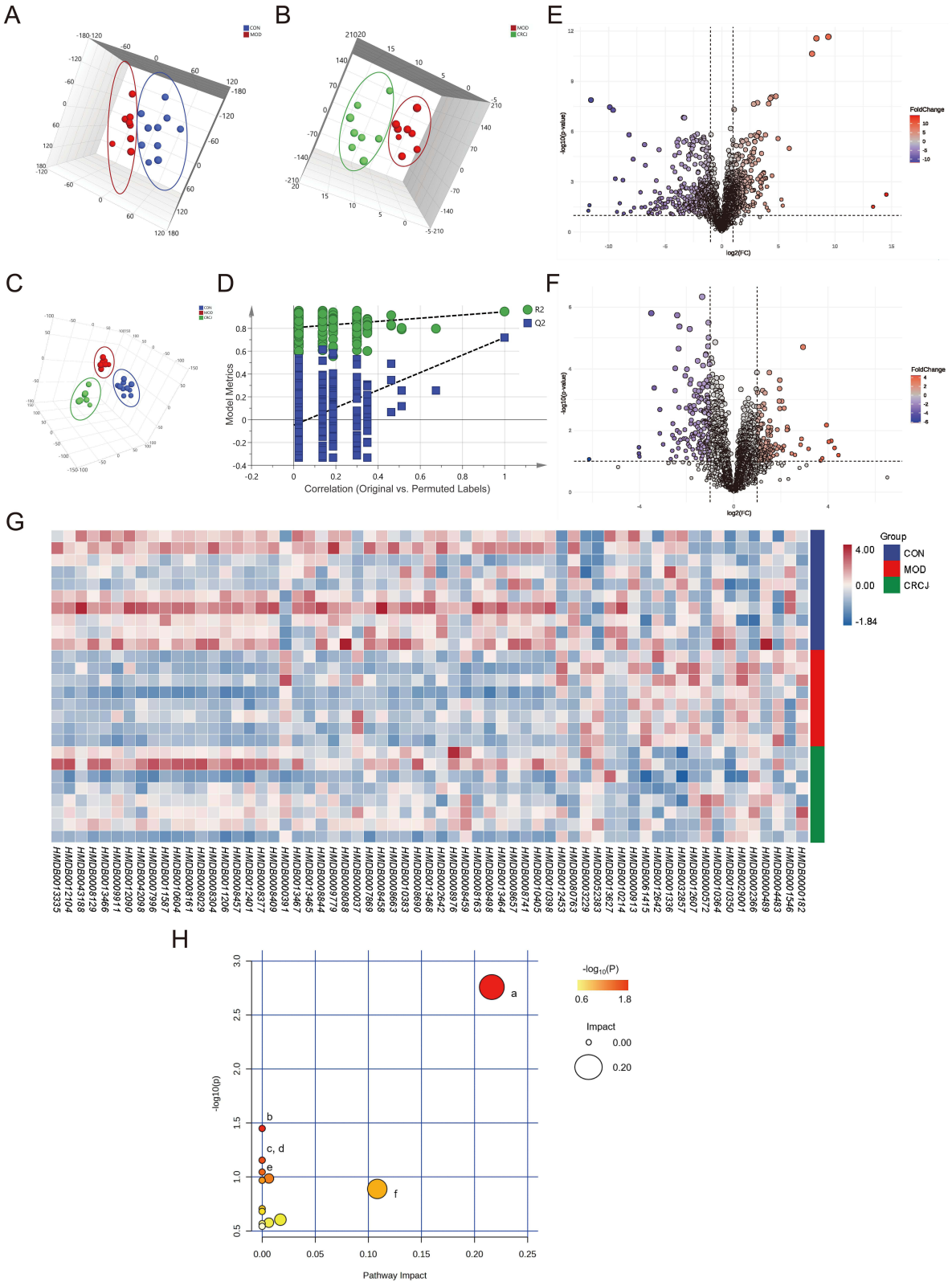

Figure 5 CRCJ regulated metabolic disorders in NOD mice. (**A** and **B**) 3D plots of PCA results. (**C**) 3D plot of PLS-DA result of CON, MOD, and CRCJ group. (**D**) Cross-validation results of the PLS-DA model (200 permutations). X-axis: 0 = fully randomized labels, 1 = original, unpermuted labels. Y-axis: model metrics: R^2 (green circles, explained variance) and Q^2 (blue squares, predictive ability). Dashed lines show regression trends for permuted R^2 and Q^2; the right-most point (correlation = 1) denotes the original model. (**E** and **F**) Volcano plots of potential differential metabolites (**E**, MOD vs CON; **F**, CRCJ vs MOD). (**G**) Heatmap of 63 differentially expressed serum metabolites. (**H**) KEGG enrichment analysis of metabolic pathway. a, Glycerophospholipid metabolism; b, Linoleic acid metabolism; c, Ascorbate and aldarate metabolism; d, Biotin metabolism; e, alpha-Linolenic acid metabolism; f, Pentose and glucuronate interconversions.

https://doi.org/10.2147/JIR.S544874

Table 5 KEGG Metabolic Pathway Analysis

No.	Pathway	P	-log(p)	Holm Adjust	FDR	Impact
1	Glycerophospholipid metabolism	0.001745	2.7581	0.13963	0.13963	0.21631
2	Linoleic acid metabolism	0.035549	1.4492	1	1	0
3	Ascorbate and aldarate metabolism	0.069946	1.1552	1	1	0
4	Biotin metabolism	0.069946	1.1552	1	1	0
5	Alpha-Linolenic acid metabolism	0.090044	1.0455	1	1	0
6	Glycosylphosphatidylinositol (GPI)-anchor biosynthesis	0.10322	0.98622	1	1	0.00639
7	Steroid hormone biosynthesis	0.1074	0.96899	1	1	0
8	Pentose and glucuronate interconversions	0.12906	0.8892	1	1	0.10843
9	Lysine degradation	0.19667	0.70627	1	1	0
10	Sphingolipid metabolism	0.20843	0.68103	1	1	0
11	Pyrimidine metabolism	0.24839	0.60486	1	1	0.0172
12	Tyrosine metabolism	0.26495	0.57684	1	1	0.00635
13	Arachidonic acid metabolism	0.27039	0.568	1	1	0
14	Primary bile acid biosynthesis	0.28651	0.54286	1	1	0

Abbreviation: FDR, false discovery rate.

Discussion

Oral and ocular dryness are the most typical symptoms of SS, affecting 98% of SS patients.[39] Inadequate glandular secretion due to immune inflammation is the most direct cause of oral dryness.[40] In the absence of ideal therapy or specific drugs, TCM has been widely applied and developed for SS treatment and has exhibited remarkable efficacy.[10,41] CRCJ is a compound preparation of 12 compatible Chinese medicines according to the theory of Monarch-Minister-Assistant-Guide (Jun-Chen-Zuo-Shi in Chinese) whose effectiveness and safety has been proven in clinical trials.[11,42] Recently, a multicenter Phase II clinical trial is underway. The present study demonstrated that CRCJ ameliorated the SS-like manifestations in NOD mice and modulated pentose and glucuronate interconversions pathway in NOD mice, which was linked to disease severity and increased Th17 cells in SS.[34] Using network pharmacology analysis, we screened core targets such as HSP90AA1, TNF, MMP9, MAPK1 (ERK2), and IL6, as well as the key pathway, IL-17 signaling pathway.

Th17 cells and their signature cytokine IL-17 play important roles in the occurrence and development of sialoadenitis (Figure 8).[30,32,43] In IL-17 signaling pathway, IL-17 induces downstream signaling through receptor complexes of specific dimer IL-17 receptor A (IL-17RA) and IL-17RC. Act1 is the adaptor protein after IL-17R binds IL-17 and is able to recruit and ubiquitinate TRAF6.[44] HSP90 maintains the integrity of Act1 so that its inhibition leads to Act1 proteasomal degradation.[45] Act1 binding to TRAF6 mediates the activation of several inflammatory pathways, including MAPK, and upregulates the expression of proinflammatory chemokines and cytokines.

An additional step in the cascade involves proteases secreted by inflammatory cells and epithelial cells that degrade ECM (Figure 8). In SS, Th17-derived IL-17 promotes recruitment of macrophages and neutrophils, which secrete MMPs and neutrophil elastase that degrade ECM proteins.[36,46] Additionally, TNF-α, IFN-α and specific IgG autoantibodies in salivary glands stimulate immune and epithelial cells to produce proteases.[47,48] ECM degradation alters acinar structure, inhibits the proliferation, differentiation, and regeneration of epithelial cells, and activates apoptosis, ultimately leading to loss of salivary-gland structure and function.[49] This aberrant tissue degradation releases soluble damage-associated molecular patterns that engage pattern recognition receptors and activate innate immunity in SS; the ensuing adaptive response can generate autoantibodies against ECM components and thereby exacerbate tissue damage.[31,50,51]

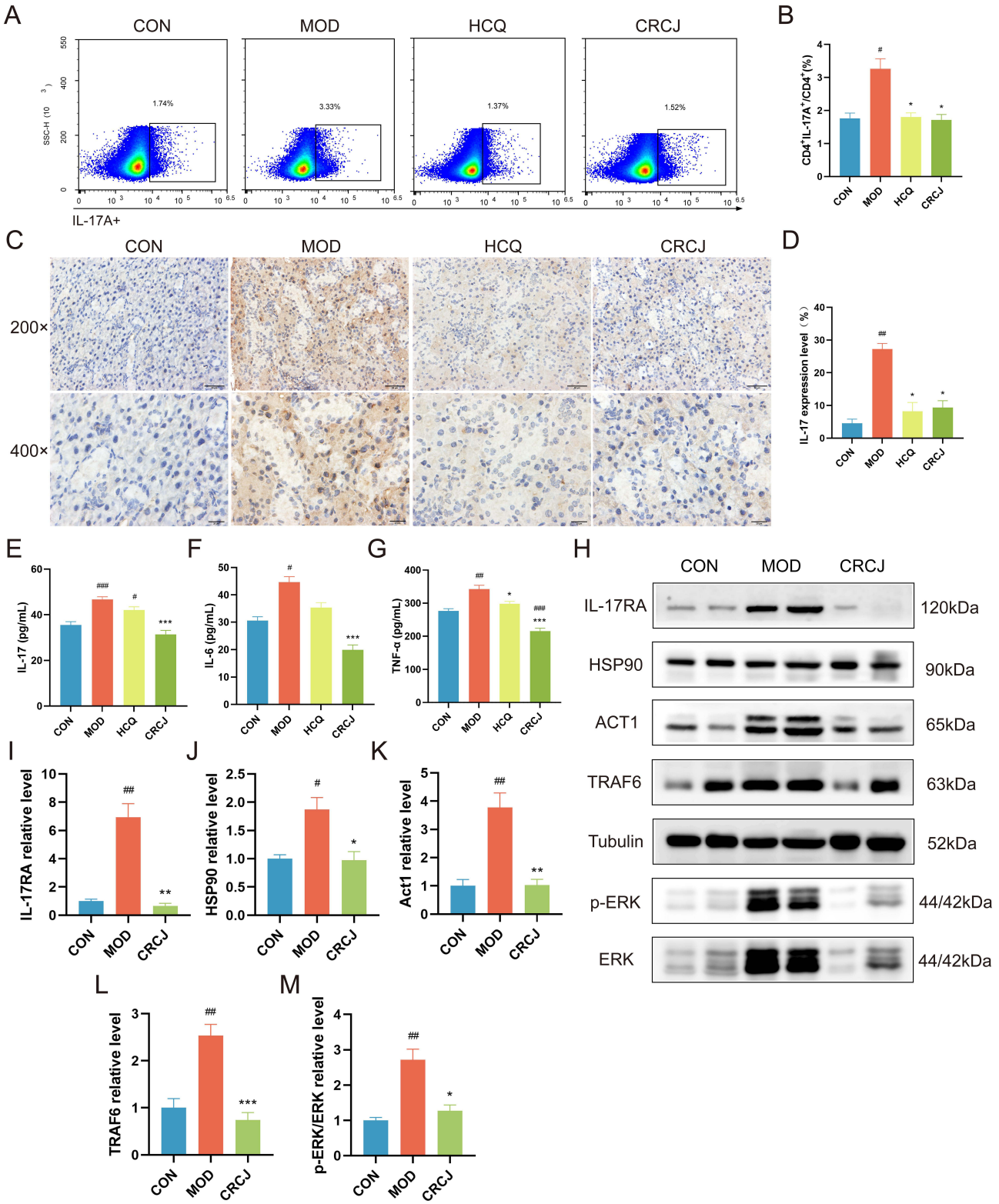

Figure 6 CRCJ inhibited Th17 cell activation and its mediated autoimmune inflammation. (**A**) The proportion of splenic Th17 cells determined by flow cytometry. (**B**) Th17 cell proportion in each group. (**C** and **D**) IHC staining of IL-17A in SMG tissues. (**E–G**) Serum IL-17, IL-6, and TNF-α levels in each group. (**H**) Western blot analysis of key proteins in IL-17 signaling pathway. (**I–M**) Statistical analysis of relative expression level of IL-17RA, HSP90, Act1, TRAF6, and p-ERK/ERK. $^{\#}$, *P<0.05, $^{\#\#}$, **P<0.01, $^{\#\#\#}$, ***P<0.001. $^{\#}$Compared with the CON group. *Compared with the MOD group.

https://doi.org/10.2147/JIR.S544874

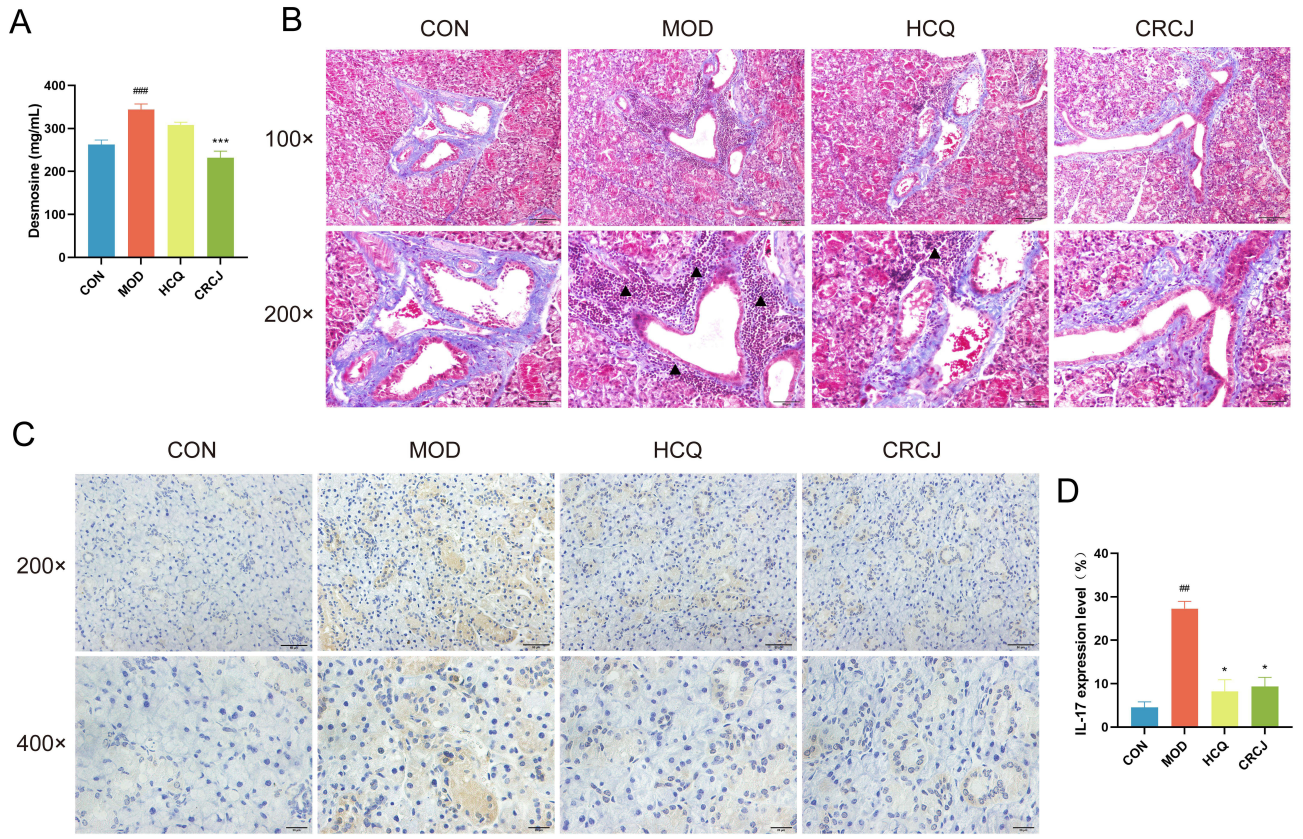

Figure 7 CRCJ protected SMG against ECM degradation. (**A**) Serum desmosine levels in each group. (**B**) Masson staining of SMG tissues. Blue-purple collagen fibers around glandular ducts and blood vessels were disrupted by inflammatory infiltration (▲). (**C** and **D**) IHC staining of SMG to detect MMP-9 expression level. **P*<0.05, ###, ****P*<0.001. #Compared with the CON group. *Compared with the MOD group.

CRCJ disrupted this vicious cycle triggered by the combination of immune inflammation and epithelial activation (Figure 8). CRCJ inhibited the activation of Th17 cells, blocked the critical site of IL-17 signaling pathway, and protected ECM structure by diminishing MMP-9 in SMG. The results emphasize the repressive effect of CRCJ on Th17 cell activation and its induced immune inflammatory cascade in SS.

UPLC-Q-TOF-MS analysis identified that CRCJ contains abundant flavonoids, which exert anti-inflammatory effects by inhibiting the secretion of inflammatory cytokines (eg, TNF-α, IL-6, IL-1β), stabilizing anti-inflammatory factors, and modulating cytokine receptors. It has been reported that puerarin, luteolin 7-O-β-D-glucoside, and diosmetin 7-O-β-D-glucoside exhibit anti-inflammatory activity and act as natural elastase and MMP inhibitors.[52,53] Rutin has been shown to improve salivation and salivary gland index in SS and displays MMP-inhibitory activities.[54,55] Molecular docking demonstrated that multiple CRCJ components bind favorably to core targets in the IL-17 signaling pathway (HSP90AA1, TNF, NFKB1, CASP3, MMP9, MAPK1, IL-6), with luteolin-7-O-β-D-glucoside, rutin, and 1,4-dicaffeoylquinic acid in particular showing strong binding affinity. Moreover, anemarsaponin C has the highest relative abundance in CRCJ. Anemarsaponins are recognized as important natural anti-inflammatory compounds that can modulate Th17 cell differentiation and increase salivary secretion in mice.[56,57] Taken together, flavonoids represented by luteolin 7-O-β-D-glucoside and rutin, together with 1,4-dicaffeoylquinic acid and anemarsaponin C, are likely the principal bioactive components mediating the therapeutic effects of CRCJ in suppressing the IL-17-induced inflammatory cascade in SS.

There are several shortcomings to consider with the current study. Mechanistic evaluation of CRCJ was limited to a spontaneous SS mouse model and lacked in vitro validation in salivary gland epithelial cells. Future work will design experiments to block the IL-17 signaling pathway to provide stronger causal evidence. Given that CRCJ is a multi-herbal complex formulation, we have identified 373 compounds across 11 herbs; however, pharmacologically active components identification remains a non-trivial challenge. Although integrative analyses have enabled the prioritization of

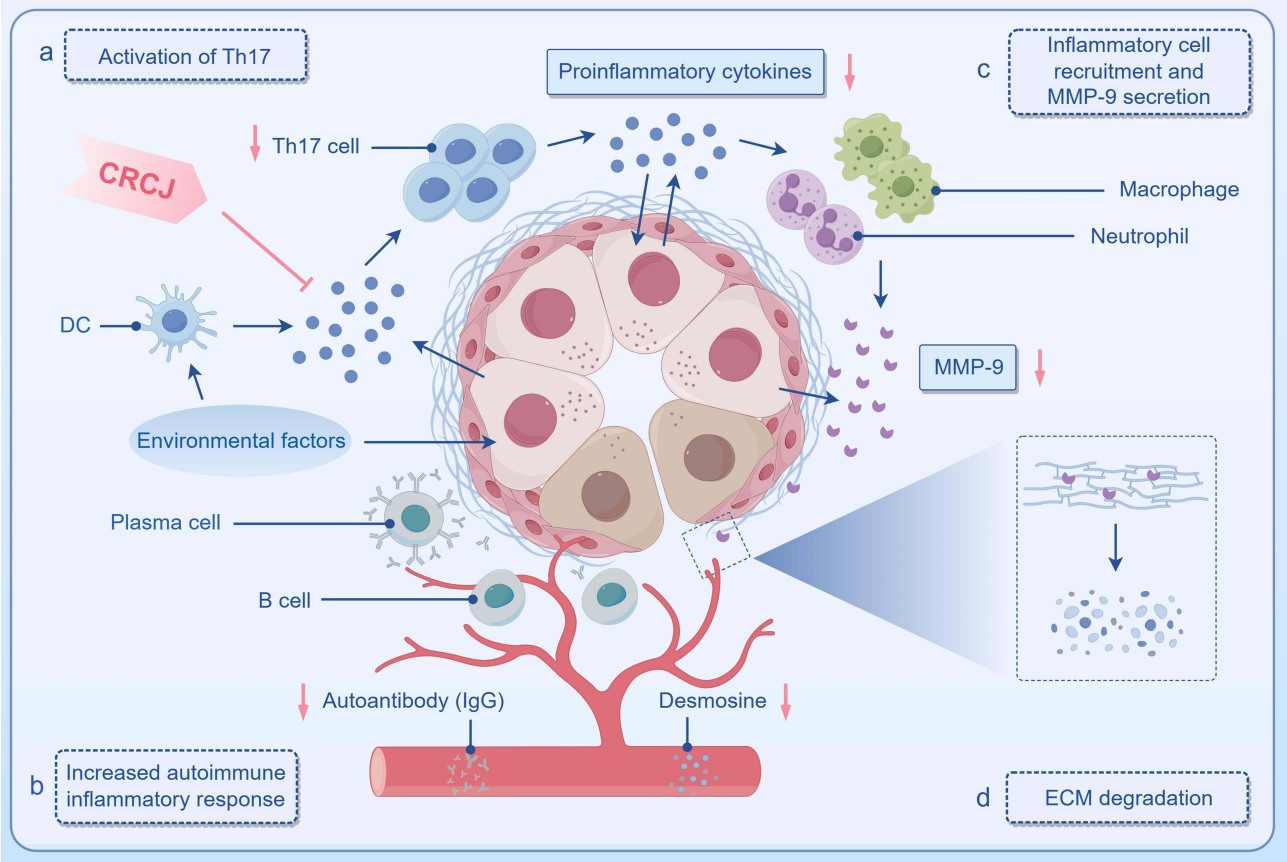

Figure 8 Potential mechanisms by which CRCJ improves SS. Normal salivary gland acini are vesicular or tubuloacinar, with many secretory granules in the apical cytoplasm, and myoepithelial cells between the glandular epithelial cells and the basement membrane to aid in the discharge of acinar secretions. The peripheral ECM maintains the structural stability of acini. In SS, (**a**) environmental factors stimulate the cells to secrete proinflammatory cytokines and present antigens, leading to Th17 cell activation. (**b**) Activated Th17 cells stimulate the release of proinflammatory cytokines from inflamed glandular epithelial cells through the secretion of IL-17 and IL-22, exacerbating inflammation. (**c**) Th17 cells and their cytokines recruit macrophages and neutrophils to sites of inflammation to secrete MMP-9. (**d**) MMP-9 degrades the ECM resulting in structural instability of the acini and apoptosis of glandular epithelial cells. CRCJ may alleviate SS by downregulating Th17 cell activation, IL-17 secretion, and the inflammatory cascade triggered by them. Blue →: activation or upregulation; pink →: downregulation; pink ⊥: inhibition.

luteolin 7-O-β-D-glucoside, rutin, 1,4-dicaffeoylquinic acid, and anemarsaponin C, further pharmacokinetic investigations and mechanistic validations are required to establish their safety and regulatory effects on the IL-17 signaling pathway in SS. High-throughput untargeted metabolomics research has a broad scope, but its quantitative results are relative. Differential metabolites except desmosine were simply labelled as potential biomarkers. The association signals between differential metabolites and KEGG pathways were generally weak, which exhibit limited biological significance. Targeted validation and more stringent screening approaches could be incorporated into subsequent confirmatory studies.

Conclusion

This study revealed that CRCJ improved the phenotype of SS sialoadenitis and ameliorated metabolic disorders in NOD mice. CRCJ downregulated IL-17-mediated inflammatory cascade, thereby exerting a protective effect on the salivary glands. Flavonoids represented by luteolin 7-O-glucoside and rutin, together with 1,4-dicaffeoylquinic acid and anemarsaponin C, are presumably the main pharmacologically active components of CRCJ, though further experimental validation is required. This work offers novel insights into traditional medicine and provides a scientific foundation for developing CRCJ or its components as promising therapeutic candidates.

Data Sharing Statement

Data will be made available from the corresponding author (Prof. Bin Wu, wuubinn@126.com) upon request.

Ethics Statement

This study followed the Guide for the Care and Use of Laboratory Animals and was approved by the Ethical Committee of Guangdong Provincial Hospital of Chinese Medicine (also known as The Second Clinical College of Guangzhou University of Chinese Medicine, Guangzhou, China) on July 21, 2022 (approval no. 2022063).

Author Contributions

All authors made a significant contribution to the work reported, whether that is in the conception, study design, execution, acquisition of data, analysis and interpretation, or in all these areas; took part in drafting, revising or critically reviewing the article; gave final approval of the version to be published; have agreed on the journal to which the article has been submitted; and agree to be accountable for all aspects of the work.

Funding

This work was supported by the Chinese Medicine Research Program of Chongqing Municipal Health and Health Committee and Chongqing Science and Technology Commission (2023DBXM009) and the Open Research Project of Chongqing Key Laboratory of Traditional Chinese Medicine to Prevent and Treat Autoimmune Diseases (ZDSYS-KF-2021-1).

Disclosure

The authors declare that they have no known competing financial interests or personal relationships that could have appeared to influence the work reported in this paper.

References

1. Beydon M, McCoy S, Nguyen Y, Sumida T, Mariette X, Seror R. Epidemiology of Sjögren syndrome. *Nat Rev Rheumatol*. 2024;20(3):158–169. doi:10.1038/s41584-023-01057-6
2. Zhang NZ, Shi CS, Yao QP, et al. Prevalence of primary Sjögren's syndrome in China. *J Rheumatol*. 1995;22(4):659–661.
3. Xiang YJ, Dai SM. Prevalence of rheumatic diseases and disability in China. *Rheumatol Int*. 2009;29(5):481–490. doi:10.1007/s00296-008-0809-z
4. Mavragani CP, Moutsopoulos HM. Sjögren's syndrome. *Annu Rev Pathol*. 2014;9:273–285. doi:10.1146/annurev-pathol-012513-104728
5. Vivino FB, Bunya VY, Massaro-Giordano G, et al. Sjogren's syndrome: an update on disease pathogenesis, clinical manifestations and treatment. *Clin Immunol*. 2019;203:81–121. doi:10.1016/j.clim.2019.04.009
6. Brito-Zerón P, Baldini C, Bootsma H, et al. Sjögren syndrome. *Nat Rev Dis Primers*. 2016;2:16047. doi:10.1038/nrdp.2016.47
7. Seror R, Nocturne G, Mariette X. Current and future therapies for primary Sjögren syndrome. *Nat Rev Rheumatol*. 2021;17(8):475–486. doi:10.1038/s41584-021-00634-x
8. Mavragani CP, Moutsopoulos HM. Sjögren's syndrome: old and new therapeutic targets. *J Autoimmun*. 2020;110:102364. doi:10.1016/j.jaut.2019.102364
9. Luo H, Li X, Liu J, Andrew F, George L. Chinese Herbal Medicine in Treating Primary Sjögren's Syndrome: a Systematic Review of Randomized Trials. *Evid Based Complement Alternat Med*. 2012;2012:640658. doi:10.1155/2012/640658
10. Wei SJ, He QM, Zhang Q, et al. Traditional Chinese medicine is a useful and promising alternative strategy for treatment of Sjogren's syndrome: a review. *J Integr Med*. 2021;19(3):191–202. doi:10.1016/j.joim.2021.01.008
11. Shao Q, Jin L, Li C, et al. Comparative analysis of the efficacy and safety of herbal decoction CheReCunJin alone and combined with hydroxychloroquine for treating primary Sjögren's syndrome: a randomized controlled trial. *Explore*. 2022;18(4):416–422. doi:10.1016/j.explore.2021.08.002
12. Wu H, Chen X, Gu F, et al. CP-25 alleviates antigen-induced experimental Sjögren's syndrome in mice by inhibiting JAK1-STAT1/2-CXCL13 signaling and interfering with B-cell migration. *Lab Invest*. 2021;101(8):1084–1097. doi:10.1038/s41374-020-0453-0
13. Chisholm DM, Waterhouse JP, Mason DK. Lymphocytic sialadenitis in the major and minor glands: a correlation in postmortem subjects. *J Clin Pathol*. 1970;23(8):690–694. doi:10.1136/jcp.23.8.690
14. Cutler LS, Rozenski D, Coolens J, et al. Experimental autoallergic sialadenitis in the LEW rat. I. Parameters of disease induction. *Cell Immunol*. 1991;135(2):335–345. doi:10.1016/0008-8749(91)90278-j
15. Li Y, Yang X, Zhang Q, et al. Dynamics of physicochemical properties, volatile aroma compounds and non-volatile metabolites of Zhaiji millet vinegar during aging: a systematic elucidation by GC-IMS coupled with UPLC-MS/MS untargeted metabolomics. *Food Chem*. 2025;493(Pt 4):146009. doi:10.1016/j.foodchem.2025.146009
16. Lee HK, Kim K, Lee J, et al. Targeted toxicometabolomics of endosulfan sulfate in adult zebrafish (Danio rerio) using GC-MS/MS in multiple reaction monitoring mode. *J Hazard Mater*. 2020;389:122056. doi:10.1016/j.jhazmat.2020.122056
17. Hwang SH, Park JS, Yang S, et al. Metabolic abnormalities exacerbate Sjögren's syndrome by and is associated with increased the population of interleukin-17-producing cells in NOD/ShiLtJ mice. *J Transl Med*. 2020;18(1):186. doi:10.1186/s12967-020-02343-7
18. Xu J, Shen Z, Du Y, et al. Huoxue Jiedu Recipe represses mitochondrial fission to alleviate submandibular gland inflammation in Sjögren's syndrome. *Microbiol Immunol*. 2023;67(8):377–387. doi:10.1111/1348-0421.13084
19. Wang Y, Yan T, Shen J, Guo H, Xiang X. Preventive effect of Ophiopogon japonicus polysaccharides on an autoallergic mouse model for Sjogren's syndrome by regulating the Th1/Th2 cytokine imbalance. *J Ethnopharmacol*. 2007;114(2):246–253. doi:10.1016/j.jep.2007.08.014

20. Mavragani CP. Mechanisms and New Strategies for Primary Sjögren's Syndrome. *Annu Rev Med*. 2017;68:331–343. doi:10.1146/annurev-med-043015-123313
21. Zhang R, Yang M, Hou X, et al. Characterization and difference of lipids and metabolites from Jianhe White Xiang and Large White pork by high-performance liquid chromatography-tandem mass spectrometry. *Food Res Int*. 2022;162(Pt A):111946. doi:10.1016/j.foodres.2022.111946
22. Zhou Y, Li R, Zheng Y, et al. Diosgenin Ameliorates Non-alcoholic Fatty Liver Disease by Modulating the Gut Microbiota and Related Lipid/Amino Acid Metabolism in High Fat Diet-Fed Rats. *Front Pharmacol*. 2022;13:854790. doi:10.3389/fphar.2022.854790
23. Wang Q, Xu K, Cai X, Wang C, Cao Y, Xiao J. Rosmarinic Acid Restores Colonic Mucus Secretion in Colitis Mice by Regulating Gut Microbiota-Derived Metabolites and the Activation of Inflammasomes. *J Agric Food Chem*. 2023;71(11):4571–4585. doi:10.1021/acs.jafc.2c08444
24. Hasegawa H, Lei J, Matsumoto T, Onishi S, Suemori K, Yasukawa M. Lysophosphatidylcholine enhances the suppressive function of human naturally occurring regulatory T cells through TGF-β production. *Biochem Biophys Res Commun*. 2011;415(3):526–531. doi:10.1016/j.bbrc.2011.10.119
25. Carneiro AB, Iaciura BMF, Nohara LL, et al. Lysophosphatidylcholine Triggers TLR2- and TLR4-Mediated Signaling Pathways but Counteracts LPS-Induced NO Synthesis in Peritoneal Macrophages by Inhibiting NF-κB Translocation and MAPK/ERK Phosphorylation. *PLoS One*. 2013;8(9):e76233. doi:10.1371/journal.pone.0076233
26. Askari AA, Thomson S, Edin ML, et al. Basal and inducible anti-inflammatory epoxygenase activity in endothelial cells. *Biochem Biophys Res Commun*. 2014;446(2):633–637. doi:10.1016/j.bbrc.2014.03.020
27. Simard M, Grenier A, Rioux G, et al. Remodeling of the Dermal Extracellular Matrix in a Tissue-Engineered Psoriatic Skin Model by n-3 Polyunsaturated Fatty Acids. *Biomedicines*. 2022;10(5):1078. doi:10.3390/biomedicines10051078
28. Campos MA, Geraghty P, Holt G, et al. The Biological Effects of Double-Dose Alpha-1 Antitrypsin Augmentation Therapy. A Pilot Clinical Trial. *Am J Respir Crit Care Med*. 2019;200(3):318–326. doi:10.1164/rccm.201901-0010OC
29. Thomas J, Elsden DF, Partridge SM. PARTIAL STRUCTURE OF TWO MAJOR DEGRADATION PRODUCTS FROM THE CROSS-LINKAGES IN ELASTIN. *Nature*. 1963;200:651–652. doi:10.1038/200651a0
30. García-Carrasco M, Fuentes-Alexandro S, Escárcega RO, Salgado G, Riebeling C, Cervera R. Pathophysiology of Sjögren's syndrome. *Arch Med Res*. 2006;37(8):921–932. doi:10.1016/j.arcmed.2006.08.002
31. Schenke-Layland K, Xie J, Angelis E, et al. Increased degradation of extracellular matrix structures of lacrimal glands implicated in the pathogenesis of Sjögren's syndrome. *Matrix Biol*. 2008;27(1):53–66. doi:10.1016/j.matbio.2007.07.005
32. Verstappen GM, Corneth OBJ, Bootsma H, Kroese FGM. Th17 cells in primary Sjögren's syndrome: pathogenicity and plasticity. *J Autoimmun*. 2018;87:16–25. doi:10.1016/j.jaut.2017.11.003
33. Mariamenatu AH, Abdu EM. Overconsumption of Omega-6 Polyunsaturated Fatty Acids (PUFAs) versus Deficiency of Omega-3 PUFAs in Modern-Day Diets: the Disturbing Factor for Their "Balanced Antagonistic Metabolic Functions" in the Human Body. *J Lipids*. 2021;2021:8848161. doi:10.1155/2021/8848161
34. Xin X, Wang Q, Qing J, et al. Th17 cells in primary Sjögren's syndrome negatively correlate with increased Roseburia and Coprococcus. *Front Immunol*. 2022;13:974648. doi:10.3389/fimmu.2022.974648
35. Foraida ZI, Kamaldinov T, Nelson DA, Larsen M, Castracane J. Elastin-PLGA hybrid electrospun nanofiber scaffolds for salivary epithelial cell self-organization and polarization. *Acta Biomater*. 2017;62:116–127. doi:10.1016/j.actbio.2017.08.009
36. Gliozzi M, Greenwell-Wild T, Jin W, et al. A link between interferon and augmented plasmin generation in exocrine gland damage in Sjögren's syndrome. *J Autoimmun*. 2013;40:122–133. doi:10.1016/j.jaut.2012.09.003
37. Fei Y, Zhang W, Lin D, et al. Clinical parameter and Th17 related to lymphocytes infiltrating degree of labial salivary gland in primary Sjögren's syndrome. *Clin Rheumatol*. 2014;33(4):523–529. doi:10.1007/s10067-013-2476-z
38. Wang X, Zhang Y, Chang X, et al. The Inhibitory Effect of the Active Ingredients in the Bushen Huoxue Formula on the IL-17A Signaling Pathway and Its Alleviating Effect on Osteoarthritis. *J Inflamm Res*. 2025;18:6505–6527. doi:10.2147/JIR.S506716
39. Negrini S, Emmi G, Greco M, et al. Sjögren's syndrome: a systemic autoimmune disease. *Clin Exp Med*. 2022;22(1):9–25. doi:10.1007/s10238-021-00728-6
40. Hu J, Andablo-Reyes E, Mighell A, Pavitt S, Sarkar A. Dry mouth diagnosis and saliva substitutes-A review from a textural perspective. *J Texture Stud*. 2021;52(2):141–156. doi:10.1111/jtxs.12575
41. Yu MC, Lin SK, Lai JN, Wei JCC, Cheng CY. The traditional Chinese medicine prescription patterns of Sjögren's patients in Taiwan: a population-based study. *J Ethnopharmacol*. 2014;155(1):435–442. doi:10.1016/j.jep.2014.05.049
42. Luan X, Zhang LJ, Li XQ, et al. Compound-based Chinese medicine formula: from discovery to compatibility mechanism. *J Ethnopharmacol*. 2020;254:112687. doi:10.1016/j.jep.2020.112687
43. Mavragani CP, Moutsopoulos HM. The geoepidemiology of Sjögren's syndrome. *Autoimmun Rev*. 2010;9(5):A305–310. doi:10.1016/j.autrev.2009.11.004
44. Amatya N, Garg AV, Gaffen SL. IL-17 Signaling: the Yin and the Yang. *Trends Immunol*. 2017;38(5):310–322. doi:10.1016/j.it.2017.01.006
45. Wu L, Wang C, Boisson B, et al. The differential regulation of human ACT1 isoforms by Hsp90 in IL-17 signaling. *J Immunol*. 2014;193(4):1590–1599. doi:10.4049/jimmunol.1400715
46. Mortensen JH, Manon-Jensen T, Jensen MD, et al. Ulcerative colitis, Crohn's disease, and irritable bowel syndrome have different profiles of extracellular matrix turnover, which also reflects disease activity in Crohn's disease. *PLoS One*. 2017;12(10):e0185855. doi:10.1371/journal.pone.0185855
47. Maciejczyk M, Pietrzykowska A, Zalewska A, Knaś M, Daniszewska I. The Significance of Matrix Metalloproteinases in Oral Diseases. *Adv Clin Exp Med*. 2016;25(2):383–390. doi:10.17219/acem/30428
48. Sembler-Møller ML, Belstrøm D, Locht H, Pedersen AML. Proteomics of saliva, plasma, and salivary gland tissue in Sjögren's syndrome and non-Sjögren patients identify novel biomarker candidates. *J Proteomics*. 2020;225:103877. doi:10.1016/j.jprot.2020.103877
49. Ram M, Sherer Y, Shoenfeld Y. Matrix metalloproteinase-9 and autoimmune diseases. *J Clin Immunol*. 2006;26(4):299–307. doi:10.1007/s10875-006-9022-6
50. Kiripolsky J, Kasperek EM, Zhu C, et al. Immune-Intrinsic Myd88 Directs the Production of Antibodies With Specificity for Extracellular Matrix Components in Primary Sjögren's Syndrome. *Front Immunol*. 2021;12:692216. doi:10.3389/fimmu.2021.692216
51. Fernandez-Ruiz R, Niewold TB. Type I IFNs in Autoimmunity. *J Invest Dermatol*. 2022;142(3 Pt B):793–803. doi:10.1016/j.jid.2021.11.031

52. Jeon YD, Lee JH, Lee YM, Kim DK. Puerarin inhibits inflammation and oxidative stress in dextran sulfate sodium-induced colitis mice model. *Biomed Pharmacother*. 2020;124:109847. doi:10.1016/j.biopha.2020.109847
53. Ma TW, Wen YJ, Song XP, et al. Puerarin inhibits the development of osteoarthritis through antiinflammatory and antimatrix-degrading pathways in osteoarthritis-induced rat model. *Phytother Res*. 2021;35(5):2579–2593. doi:10.1002/ptr.6988
54. Li W, Gong H, Yan S, et al. Effective Delivery of Rutin Through Astragalus Polysaccharides Micelles for Downregulating PD-L1 by Inhibiting Matrix Metalloproteinases. *ACS Appl Mater Interfaces*. 2025. doi:10.1021/acsami.5c11872
55. He J, Xu M, Wu S. Rutin alleviates Sjogren's syndrome via CaR/NLRP3/NF-κB signal pathway. *Vitro Cell Dev Biol Anim*. 2024;60(4):411–419. doi:10.1007/s11626-024-00893-4
56. Kimura M, Kimura I, Chem FJ. Combined potentiating effect of byakko-ka-ninjin-to, its constituents, rhizomes of Anemarrhena asphodeloides, tomosaponin A-III, and calcium on pilocarpine-induced saliva secretion in streptozocin-diabetic mice. *Biol Pharm Bull*. 1996;19(7):926–931. doi:10.1248/bpb.19.926
57. Wang L, Yuan J, Zhao R, Wang C, Li Z. Timosaponin A-III Alleviates Asthma-Induced Airway Inflammation, Th17 Cell Differentiation, and STAT3/RORγt Pathway. *Immunol Invest*. 2025;54(4):544–559. doi:10.1080/08820139.2025.2450239